Supporting Information: Electron Transfer Activity in a Cyanide-Bridged Fe_{42} Nanomagnet

Michael L. Baker,[*,†,‡] Shu-Qi Wu,[¶] Soonchul Kang,[§] Satoshi Matsuzawa,[‖] Marie-Anne Arrio,[⊥] Yasuo Narumi,[#] Takumi Kihara,[‖] Tetsuya Nakamura,[@] Yoshinori Kotani,[@] Osamu Sato,[*,¶] and Hiroyuki Nojiri[*,‖]

†*The School of Chemistry, The University of Manchester at Harwell, Didcot, OX11 OFA, UK.*

‡*The School of Chemistry, The University of Manchester, M139PL, Manchester, UK.*

¶*Institute for Materials Chemistry and Engineering, Kyushu University, 744 Motooka, Nishi-ku, Fukuoka, 819-0395, Japan.*

§*Department of Chemical Engineering, Graduate School of Engineering, Hiroshima University, 1-4-1, Kagamiyama, Higashihiroshima, Hiroshima, 739-8527, Japan.*

‖*Institute for Materials Research, Tohoku University, Katahira, Sendai 980-8577, Japan.*

⊥*Institut de Minéralogie, de Physique des Matériaux et de Cosmochimie, CNRS, Sorbonne Université, IRD, MNHN, UMR7590, 75252 Paris Cedex 05, France.*

#*Center of Advanced High Magnetic Field Science, Osaka University, Toyonaka 1-1, Osaka 560-0043, Japan.*

@*Japan Synchrotron Radiation Research Institute (JASRI), Sayo, Hyogo 679-5198, Japan.*

E-mail: michael.baker@manchester.ac.uk; sato@cm.kyushu-u.ac.jp; nojiri@imr.tohoku.ac.jp

Specific Heat Capacity

Since molecular clusters with large spin moments can exhibit dipolar field driven three dimensional ordering,[1–4] we measured the low temperature specific heat capacity of Fe_{42} and confirmed that the S=45 ground state is molecular in origin. Specific heat capacity measurements down to 0.5 K (Figure S1) do not show the appearance of a λ-type anomaly associated with a magnetic phase transition. A broad shoulder deviating from the lattice contribution to the specific heat is observed in zero field at 5 K, consistent with a Schottky anomaly, associated with weak exchange coupling within the molecule. The application of an applied field of 1 T sees this broad feature shift up to 8 K in accordance with the Zeeman-effect. A lack of evidence of anisotropy induced zero-field splitting, confirms the isotropic nature of the S=45 ground state, a result of the cluster's symmetry.

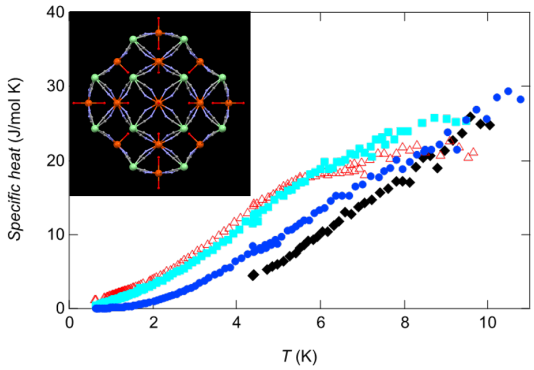

Figure S1: Specific heat capacity of polycrystalline Fe_{42} measured at 0 T (red triangles), 1 T (blue squares), 5 T (blue circles) and 10 T (black diamonds). Insert: Fe_{42} skeleton crystal structure. The 24 $\{Fe(Tp)(CN)_3\}$ are shown as green spheres, the $\{Fe(NC)_4(H_2O)_2\}$ and $\{Fe(NC)_4(dpp)(H_2O)\}$ are shown as orange spheres with axial O atoms shown as small red spheres, C; grey spheres and N; blue spheres) and terminal ligand atoms removed clarity.

Charge Transfer Multiplet Calculations

Charge transfer multiplet simulations of XAS and XMCD are used to determine Fe ion ground states, crystal fields, and nature of metal - ligand hybridization. The calculations were implemented using the TT-multiplets suite of programs. To simulate the spectra, the

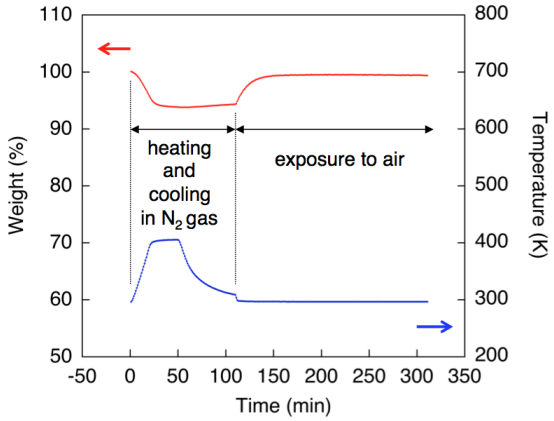

Figure S2: Thermal gravimetric analysis of Fe_{42}. A 5% weight loss is observed on heating the sample above room temperature. The lost mass is recovered on exposure of the sample to to air at room temperature.

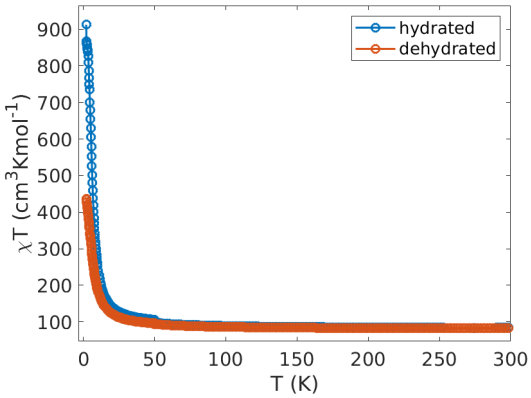

Figure S3: Magnetic susceptibility plotted as the χT product as a function of temperature for a powder sample of Fe_{42} in hydrated and dehydrated forms. A applied field of 50 Oe is applied from 2 to 50 K and 1000 Oe from 51 K to 300 K.

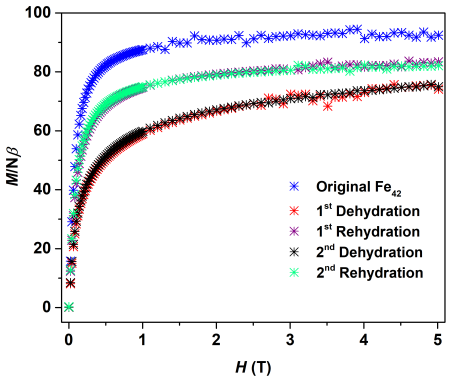

Figure S4: Magnetisation as a function of external magnetic field for a powder sample of Fe_{42} during two dehydration-rehydration cycles at 2 K.

Slater-Condon-Shortley parameters, the radial (F^i and G^i) and angular part (f^i and g^i) of Coulomb repulsion and Coulomb exchange interaction, were reduced and fixed to 80% of their Hartree-Fock calculated values in order to account for the overestimation of electron-electron repulsion found in the calculations of the free ion. Ligand-metal hybridisation was modelled using the valence bond configuration interaction approach with charge transfer pathways differentiated according to $3d$ orbital symmetry, as outlined in the main text.

Simulations of Reference Spectra

The XAS simulation of $K_2[Fe^{II}(Tp)(CN)_3]$ and $Li[Fe^{III}(Tp)(CN)_3]$ reference spectra were performed in O_h crystal field symmetry, where the $10Dq$ free parameter defines the energy separation between e_g and t_{2g} orbitals. Ligand-metal hybridization was simulated using metal to ligand charge transfer (MLCT) via the t_{2g} orbital symmetry ($T_{M,t_{2g}}$) and ligand to metal charge transfer via the e_g orbital symmetry (T_{L,e_g}). In the case of $Li[Fe^{III}(Tp)(CN)_3]$ XAS calculations include LMCT hybridization term is also included via t_{2g} orbital ($T_{L,t_{2g}}$) to account for delocalisation of ligand p orbital character into the t_{2g} hole. The energy separating the charge transfer configurations are Δ and Δ^* for LMCT and MLCT respectively. The parameters obtained fitting the $K_2[Fe^{II}(Tp)(CN)_3]$ and $Li[Fe^{III}(Tp)(CN)_3]$ reference spectra (table S1) were fixed for the simulation of Fe_{42} XAS spectra. XMCD simulations of

$Li[Fe^{III}(Tp)(CN)_3]$ were performed using the model and parameters previously adopted in Ref. 5.

Simulations of Fe_{42}

The 24 $Fe(Tp)(CN)_3$ sites in Fe_{42} are chemically identical to the reference compounds $K_2[Fe^{II}(Tp)(CN)_3]$ and $Li[Fe^{III}(Tp)(CN)_3]$. The remaining 18 sites do not exist as mononuclear compounds, 6 $\{Fe(NC)_4(H_2O)_2\}$ and 12 $\{Fe(NC)_4(dpp)(H_2O)\}$ (together, abbreviated as $\{FeNC_4\}$). The two moieties are very similar making differentiation of the two species in Fe_{42} unjustifiable. The XMCD of Fe_{42} indicates the presence of both Fe(II) and Fe(III) high-spin species amongst the 18 $\{FeNC_4\}$ ensemble. Initial simulations were performed with all 18 $\{FeNC_4\}$ as Fe(III), a parameter space including a broad range of both crystal field, hybridization terms and the charge transfer energy parameters do not fit the double L_3 XMCD feature or the XAS suitably. A second attempt fixed $\{FeNC_4\}$ valences to 6 $\{Fe^{II}NC_4\}$ and 12 $\{Fe^{III}NC_4\}$, in this case the double negative peaks in the L_3 XMCD could be reproduced, but with incorrect intensity ratios. Only with equal a number of Fe(II) and Fe(III) valence $\{FeNC_4\}$ is the XMCD and XAS reproduced.

The nitrogen end cyanide ligation does not exhibit sizeable MLCT, hence the inclusion of LMCT type hybridization is sufficient.[6] The $\{Fe^{III}NC_4\}$ sites include hybridization via two corresponding $T_{L,t_{2g}}$ and T_{L,e_g} terms. To obtain the best fit of XMCD and XAS an additional crystal field parameter Ds is added to the simulation of $\{Fe^{II}NC_4\}$ which distort the energy of the 3d orbitals to C_{4v}. This distortion is consistent with a reduced coordination number due to the loss of axial water molecules. The energy of the orbitals with respect to the $10Dq$ and Ds parameters are as follows:

$$
\begin{aligned}
b_1(d_{x2y2}) &= 6Dq + 2Ds \\
a_1(d_{z2}) &= 6Dq - 2Ds \\
b_2(d_{xy}) &= -4Dq + 2Ds \\
e(d_{xz,yz}) &= -4Dq - Ds.
\end{aligned}
$$

Table S1: Parameters for XAS charge transfer multiplet simulations of {FeTp} reference samples.

compound	10Dq (eV)	$T_{L,t_{2g}}$	T_{L,e_g}	$T_{M,t_{2g}}$	Δ (eV)	Δ^* (eV)
$K_2[Fe^{II}(Tp)(CN)_3]$	1.9706	-	1.0505	1.7845	-3.3839	-2.4997
$Li[Fe^{III}(Tp)(CN)_3]$	2.9597	0.8808	1.7859	1.7284	-3.4340	0.8710

Table S2: Parameters for XAS and XMCD charge transfer multiplet simulations of high spin Fe sites in Fe_{42}.

Moiety	10Dq (eV)	Ds (eV)	T_{L,b_1} (d_{x2y2})	T_{L,a_1} (d_{z2})	T_{L,b_2} (d_{xy})	$T_{L,e}$ ($d_{xz,yz}$)	Δ (eV)
$\{Fe^{II}NC_3\}$	0.8	0.05	0.2678	0.0000	0.08520	0.0000	0
$\{Fe^{III}NC_3\}$	1.2	0.00	0.7810	0.7809	0.55515	0.5551	-1

XAS Data Reduction

Figure S5 shows both left and right circularly polarized XAS and XMCD of Fe_{42}. Before fitting the measured XAS spectra a linear background function was subtracted from each averaged data set and two arctangent functions of the form absorption $I(energy) = tan^{-1}[k(energy - L_3) + \pi/2](2/3)(1/\pi) + tan^{-1}[k(energy - L_2) + \pi/2](1/3)(1/\pi)$, where k = 0.295 and $L_2 = L_3 + 12.3eV$ (energy split by $2p^5$ spin-orbit coupling), were used to model the L_3 and L_2 edge jumps.

Radiation damage due to x-ray overexposure is limited by use of a shutter system reducing exposure for each incident x-ray energy to 200 ms. With sequential reduction of the incident

x-ray flux, short scans over the the L_3-edge were repeated over the same sample spot to confirm that the spectra were not affected by damaged species contributions. Additionally, reduction of the sample temperature to < 200 K was found to reduce sample damage effects.

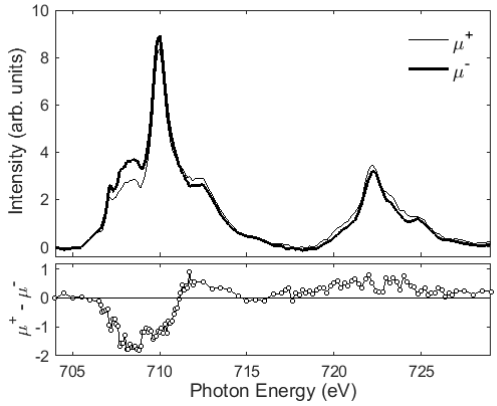

Figure S5: The circularly polarized $L_{2,3}$-edge XAS (BL25SU, SPring-8) of Fe_{42} (Top panel) and XMCD ($\mu^+ - \mu^-$) (bottom panel). The measurements were performed at 15 K with an an applied field of 1.9 T.

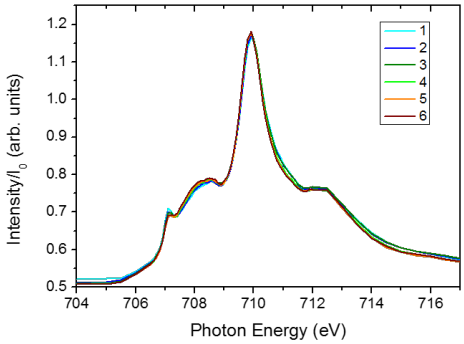

Figure S6: L_3-edge XAS (BL25SU, SPring-8) of Fe_{42} ($\mu^+ + \mu^-$) 1 to 6 are repeat measurements on the same sample spot indicating control of x-ray damage.

References

(1) Larionova, J.; Gross, M.; Pilkington, M.; Andres, H.; Stoeckli-Evans, H.; Güdel, H. U.; Decurtins, S. High-Spin Molecules: A Novel Cyano-Bridged Mn Molecular Cluster with

a S=51/2 Ground State and Ferromagnetic Intercluster Ordering at Low Temperatures. *Angew. Chem. Int. Ed.* **2000**, *39*, 1605–1609.

(2) Evangelisti, M.; Candini, A.; Ghirri, A.; Affronte, M.; Powell, G. W.; Gass, I. A.; Wood, P. A.; Parsons, S.; Brechin, E. K.; Collison, D.; Heath, S. L. Tunable Dipolar Magnetism in High-Spin Molecular Clusters. *Phys. Rev. Lett.* **2006**, *97*, 167202.

(3) Pratt, F. L.; Micotti, E.; Carretta, P.; Lascialfari, A.; Arosio, P.; Lancaster, T.; Blundell, S. J.; Powell, A. K. Dipolar ordering in a molecular nanomagnet detected using muon spin relaxation. *Phys. Rev. B* **2014**, *89*, 144420.

(4) Schnack, J. Influence of intermolecular interactions on magnetic observables. *Phys. Rev. B* **2016**, *93*, 054421.

(5) Jafri, S. F.; Koumousi, E. S.; Sainctavit, P.; Juhin, A.; Schuler, V.; Bunău, O.; Mitcov, D.; Dechambenoit, P.; Mathonière, C.; Clérac, R.; Otero, E.; Ohresser, P.; Cartier dit Moulin, C.; Arrio, M.-A. Large Orbital Magnetic Moment Measured in the [TpFeIII(CN)3] Precursor of Photomagnetic Molecular Prussian Blue Analogues. *Inorg. Chem.* **2016**, *55*, 6980–6987.

(6) Arrio, M.-A.; Sainctavit, P.; Cartier dit Moulin, C.; Mallah, T.; Verdaguer, M.; Pellegrin, E.; Chen, C. T. Characterization of Chemical Bonds in Bimetallic Cyanides Using X-ray Absorption Spectroscopy at L2,3 Edges. *J. Am. Chem. Soc.* **1996**, *118*, 6422–6427.